Inorganica Chimica Acta, 215 (1994) 123–129

Synthesis, crystal and molecular structures, UV–Vis spectroscopy and electrochemical properties of two iron(III) phenolate complexes

Marcel Lubben, Auke Meetsma, Fré van Bolhuis and Ben L. Feringa*

Department of Organic and Molecular Inorganic Chemistry, Groningen Center for Catalysis and Synthesis, University of Groningen, Nijenborgh 4, 9747 AG Groningen (Netherlands)

Ronald Hage

Unilever Research Laboratories, Olivier van Noortlaan 120, 3133 AT Vlaardingen (Netherlands)

(Received May 25, 1993; revised July 30, 1993)

Abstract

The synthesis and molecular structures of two iron(III) phenolate complexes $[(L^1)FeCl]$ (**1**) and $[(L^2)_2Fe][BPh_4]$ (**2**) are described, where L^1H_2 is 2,3-dimethyl-2,3-bis(3-tert-butylsalicylideneamino)butane and L^2H is 2-(2-pyridyl)-1-salicylideneaminoethane The complexes have been characterized by analytical, spectroscopic and electrochemical methods. Complex **1** crystallizes in the orthorhombic space group $P2_12_12_1$ with $a=9.588(2)$, $b=14.722(2)$, $c=18.921(2)$ Å and $Z=4$. On the basis of 2730 unique observed reflections with $I \geqslant 2.5\sigma(I)$ the structure was refined to $R=0.039$. Complex **2** crystallizes in the monoclinic space group $P2_1/c$ with $a=15.975(1)$, $b=15.627(2)$, $c=17.773(2)$ Å, $\beta=108.43(1)°$ and $Z=4$. On the basis of 5012 unique observed reflections with $I \geqslant 3.0\sigma(I)$ the structure was refined to $R=0.049$. Complexes **1** and **2** both show quasi-reversible Fe(II)/Fe(III) redox couples at $E_{1/2}=-0.37$ and -0.25 V, respectively

Key words Crystal structures; Electrochemistry, Iron complexes, Phenolate complexes

Introduction

Iron–phenolate (mostly tyrosinate) interactions play an important role in nature. The iron–phenolate structural feature is found in a number of metalloproteins, e.g. lactoferrin [1], the transferrins [2, 3], the catechol dioxygenases [4–6] and the purple acid phosphatases [7]. Mimicking of these iron–tyrosinate proteins through the synthesis of small molecule active site analogues has proven to be very useful in providing insights into the modes of action of these enzymes. In particular, spectroscopic techniques like UV–Vis spectroscopy, resonance Raman spectroscopy, ^1H NMR spectroscopy as well as magnetic and electrochemical measurements have contributed to elucidate structural details of the iron–tyrosinate proteins. Recently, we have initiated efforts to mimic iron–tyrosinate moieties in proteins in a functional [8] as well as in a structural way. In this study we present the crystal and molecular structures of two new iron(III) phenolate model complexes **1** and **2** together with UV–Vis spectral data and electrochemical data of these complexes.

Experimental

Materials and instruments

Iron(III) chloride hexahydrate, purchased from Merck, and iron(III) nitrate nonahydrate, purchased from Baker, were used as received. Methanol was distilled from magnesium and stored over 3 Å sieves. 2,3-Dimethyl-2,3-bis(3-tert-butylsalicylideneamino)butane (L^1H_2) [9] and 2-(2-pyridyl)-1-salicylideneaminoethane (L^2H) [10] were prepared according to literature procedures

IR spectra were obtained on a Galaxy 4020 FT-IR spectrophotometer or on a Perkin-Elmer 841 IR spectrophotometer. UV–Vis spectra were obtained on a Perkin–Elmer Lambda 5 UV–Vis spectrophotometer. Elemental analyses were performed in the Microanalytical Department of this laboratory. Mass spectra (HRMS) were obtained on an AEI-MS-902 mass spectrometer. Electrochemical measurements were made

---

*Author to whom correspondence should be addressed.

SSDI 0020-1693(93)03678-4

using an EG&G Par C model 303 potentiostat with an EG&G Par 384B polarographic analyzer. A three-electrode system consisting of a glassy carbon working electrode, a platinum wire auxiliary electrode and a saturated calomel reference electrode was used. The measurements were carried out in methanol for complex **1** and in methanol/acetonitrile (1/1) for complex **2** using 0.1 M tetrabutylammonium perchlorate (TBAP) as the supporting electrolyte. The scan rate for the cyclic voltammograms was 100 mV/s

Preparation of [(L¹)FeCl] (1)

To a suspension of 2,3-dimethyl-2,3-bis(3-tert-butyl-salicylideneamino)butane (L^1H_2) (0.25 g, 0.57 mmol) in methanol (10 ml) was added $FeCl_3 \cdot 6H_2O$ (0.157 g, 0.58 mmol) dissolved in 2 ml of methanol. The mixture was refluxed for 1 h and allowed to cool to room temperature. After standing for 1 day dark red crystals, suitable for X-ray analysis, were obtained (0.13 g, 43%) *Anal.* Calc. for $C_{28}H_{38}ClFeN_2O_2$: C, 63 95; H, 7.28; Cl, 6.74; Fe, 10.62; N, 5.33. Found· C, 64.00; H, 7.40; Cl, 6.79; Fe, 10.54; N, 5.24%.

Preparation of [(L²)₂Fe][BPh₄] (2)

To a solution of 2-(2-pyridyl)-1-salicylideneamino-ethane (L^2H) (0.678 g, 3.00 mmol) in methanol (5 ml) was added solid NaOH (0.12 g, 3.00 mmol). A solution of $Fe(NO_3)_3 \cdot 9H_2O$ (0.609 g, 1.51 mmol) in methanol (5 ml) was added. The reaction mixture was stirred for 0.5 h at room temperature. An extra amount of methanol (5 ml) was added to dissolve all of the solid material. After the dropwise addition of $NaBPh_4$ (0.52 g, 1.52 mmol) the mixture was stirred for 0.5 h and a purple precipitate was obtained. The precipitate was washed with methanol and air dried yielding a purple powder (1.15 g, 93%). Crystals, suitable for X-ray analysis, were obtained by slow vapor diffusion of methanol into a solution of the complex in acetone. *Anal.* Calc. for $C_{52}H_{46}BFeN_4O_2$: C, 75.65; H, 5.62; Fe, 6.76; N, 6 79. Found: C, 75.18; H, 5.68; Fe, 6.68; N, 6.73%.

Collection and reduction of X-ray data for [(L¹)FeCl] (1) and [(L²)₂Fe][BPh₄] (2)

Suitable crystals of **1** and **2** were glued on the top of a glass fiber and transferred into the cold nitrogen stream of the low temperature unit [11] mounted on an Enraf-Nonius CAD-4F diffractometer interfaced to a VAX-11/730 computer (Mo Kα radiation, graphite monochromator). Unit cell dimensions and their standard deviations and the orientation matrix for the data collection were determined from the setting angles of 22 reflections in the range $10.18 < \theta < 19.73°$ for **1** and from the setting angles of 25 reflections in the range $9.2 < \theta < 19\ 8°$ for **2**. Crystal data and numerical details of the structure determination are given in Table 1. Three standard reflections were measured every 3 h of X-ray exposure time as check reflections for crystal deterioration and/or misalignment; no significant deterioration in intensity was observed. Intensities were corrected accordingly, for Lorentz effects and for polarization effects, but not for absorption effects. The unit cell was identified as orthorhombic space group $P2_12_12_1$ for complex **1**; for complex **2** the unit cell was identified as monoclinic, space group $P2_1/c$. The space group of the complexes was derived from the observed systematic extinctions. This choice was confirmed by the solution and the successful refinement. From a total of 3676 reflections in the range $1.08 \leqslant \theta \leqslant 27.5°$, 2730 ($I \geqslant 2.5\sigma(I)$) were used in the refinements for complex **1**. For complex **2**, 5012 reflections ($I \geqslant 3.0\sigma(I)$) from a total of 7176 reflections in the range $1 \leqslant \theta \leqslant 25°$ were used in the refinements.

Structure solution and refinement

The structure of complex **1** was solved by Patterson methods and subsequent partial structure expansion (SHELX86 [12]). The positional and anisotropic thermal displacement parameters for the non-hydrogen atoms were refined with block-diagonal least-squares procedures (CRYLSQ [13]) minimizing the function $Q = \Sigma_h[w(|F_o| - |F_c|)^2]$. A subsequent difference Fourier synthesis resulted in the location of all the hydrogen atoms, the positions of which were included in the refinement and all hydrogen atoms subsequently refined satisfactorily. Weights were introduced in the final refinement cycles. Refinement on F_o by full-matrix least-squares techniques with anisotropic thermal displacement parameters for the non-hydrogen atoms and one common isotropic thermal displacement parameter for the hydrogen atoms converged at $R_F = 0.039$ ($R_w = 0.039$) A final difference Fourier map did not show residual peaks outside the range ± 0.56 e/Å^3. The alternative absolute structure was rejected, based on the resulting higher R values ($R_F = 0.050$; $R_w = 0.052$) obtained by refinement with negative anomalous-dispersion factors ($-i\Delta f''$). Fractional atomic coordinates and equivalent isotropic thermal displacement parameters of the non-hydrogen atoms are presented in Table 2. Scattering factors [14] were corrected for anomalous dispersion [15]. All calculations were carried out on the CDC-Cyber 962-31 computer of the University of Groningen with the program packages XTAL [16], PLATON [17] (calculation of geometric data) and an extended version of the program PLUTO [18] (preparation of illustrations).

The structure of complex **2** was solved by direct methods [19]. The remaining H atoms could be revealed from a single Fourier difference synthesis based on all the non-H atoms Full-matrix least-squares of F, with

TABLE 1. Crystal data, data collection, structure solution and refinement for **1** and **2**

	1	**2**
Crystal data		
Chemical formula	$C_{28}H_{38}FeClN_2O_2$	$C_{52}H_{46}BFeN_4O_2$
Formula weight (g mol^{-1})	525 92	825 63
Crystal system	orthorhombic	monoclinic
Space group	$P2_12_12_1$	$P2_1/c$
a (Å)	9.588(2)	15 975(1)
b (Å)	14.722(2)	15.627(2)
c (Å)	18.921(2)	17.773(2)
β (°)		108.43(1)
V ($Å^3$)	2670 8(7)	4206.9(8)
Z	4	4
D_{calc} (g cm^{-3})	1.308	1.303
$F(000)$	1116	1732
μ(Mo Kα) (cm^{-1})	6.9	4 0
Approx. crystal dimension (mm)	0 18×0 18×0.25	0 40×0.30×0.25
Data collection		
Radiation	Mo Kα (0 71073 Å)	Mo Kα (0.71073 Å)
Monochromator	graphite crystal	graphite crystal
Temperature (K)	130	130
θ Range (°)	1 08–27 5	1–25
Total data	3676	7176
Unique data	3444	7176
Observed data	2730 ($I \geqslant 2.5\sigma(I)$)	5012 ($I \geqslant 3\ 0\sigma(I)$)
Refinement		
No. reflections	2730	5012
No. refined parameters	421	541
Final agreement factors		
$R_F = \Sigma(\|\|F_o\| - \|F_c\|\|)/\Sigma\|F_o\|$	0 039	0 049
$R_w = [\Sigma(w(\|F_o\| - \|F_c\|)^2)/\Sigma w\|F_o\|^2]^{1/2}$	0 039	0 050
Goodness-of-fit[a]	1.269	2.27

[a] Goodness of fit is defined as $S = [\Sigma w(|F_o| - |F_c|)^2/(m - n)]^{1/2}$ where m is the number of observed reflections and n is the number of parameters defined

unit weights, converged to a final $R = 0.049$ and $R_w = 0.050$, including 541 variable parameters, average $\Delta/\sigma = 0.02$; maximum electron density in final difference map is 0.37 e/$Å^3$, using anisotropic temperature factors for the non-H atoms and isotropic fixed temperature factors ($B = 4.0$ $Å^2$) for the H atoms. In the final refinements the H atoms were riding on their corresponding atoms at a distance of 0.97 Å. Positional parameters and their estimated standard deviations of the cation of $[(L^2)_2Fe][BPh_4]$ (**2**) are presented in Table 3. Scattering factors were taken from Cromer and Waber [20]. Anomalous dispersion effects were included in F_c: the values were those of Cromer [21]. All computations were performed on a VAX-730.

Results and discussion

Synthesis

Heating of 2,3-dimethyl-2,3-bis(3-tert-butylsalicylideneamino)butane (L^1H_2) with $FeCl_3 \cdot 6H_2O$ in methanol afforded complex **1** (eqn. (1)).

$$L^1H_2 \xrightarrow[\text{MeOH, reflux, 1 h}]{FeCl_3\ 6H_2O} \underset{\textbf{1}}{[L^1FeCl]} \qquad (1)$$

Complex **2** was prepared from the sodium salt of 2-(2-pyridyl)-1-salicylideneaminoethane (L^2) with $Fe(NO_3)_3 \cdot 9H_2O$ followed by anion exchange with $NaBPh_4$ (eqn. (2)).

$$2L^2Na \xrightarrow[\text{(ii) } NaBPh_4]{\text{(i) } Fe(NO_3)_3\ 9H_2O\text{, MeOH}} \underset{\textbf{2}}{[(L^2)_2Fe][BPh_4]} \qquad (2)$$

Molecular structure of $[(L^1)FeCl]$ (1)

X-ray analysis revealed the molecular structure of **1** shown in Fig. 1. The relevant bond lengths and angles are depicted in Table 4. The iron nucleus of **1** is coordinated to two phenolate oxygens (O(1) and O(2)) and to two imine nitrogens (N(1) and N(2)) as well as to a chlorine atom (Cl1). These five atoms of the inner coordination sphere form an essentially square pyramidal environment for the iron nucleus. The distances between the iron nucleus and the five donor-atoms closely resemble those of the unsubstituted

TABLE 2 Fractional atomic coordinates and equivalent isotropic thermal displacement parameters of [(L^1)FeCl] (**1**) for non-H atoms with e.s.d.s in parentheses. Atoms of the asymmetric unit

	x	y	z	U_{eq}^{a} (Å^2)
Fe(1)	0.55491(6)	0.52637(4)	0.04507(3)	0.0128(2)
Cl(1)	0.39099(12)	0.61466(7)	0.09434(6)	0.0227(3)
O(1)	0.4968(3)	0.50395(17)	−0.04852(16)	0.0176(8)
O(2)	0.5055(3)	0.40916(19)	0.07807(15)	0.0178(8)
N(1)	0.7066(3)	0.6125(2)	0.00082(18)	0.0133(10)
N(2)	0.7176(3)	0.5214(2)	0.11759(18)	0.0155(10)
C(1)	0.4971(5)	0.5527(3)	−0.1068(2)	0.0160(12)
C(2)	0.4006(4)	0.5344(3)	−0.1622(2)	0.0153(11)
C(3)	0.4068(5)	0.5883(3)	−0.2218(2)	0.0183(12)
C(4)	0.5034(5)	0.6583(3)	−0.2304(2)	0.0197(12)
C(5)	0.5965(5)	0.6766(3)	−0.1775(2)	0.0177(12)
C(6)	0.5939(4)	0.6248(3)	−0.1146(2)	0.0140(12)
C(7)	0.6966(5)	0.6472(3)	−0.0618(2)	0.0153(11)
C(8)	0.8183(4)	0.6465(3)	0.0496(2)	0.0151(11)
C(9)	0.8539(4)	0.5639(3)	0.0987(2)	0.0177(12)
C(10)	0.7039(5)	0.4796(3)	0.1775(2)	0.0193(12)
C(11)	0.5070(4)	0.3779(3)	0.1434(2)	0.0160(12)
C(12)	0.4193(4)	0.3018(3)	0.1620(2)	0.0173(12)
C(13)	0.4221(5)	0.2738(3)	0.2318(3)	0.0233(16)
C(14)	0.5057(5)	0.3144(3)	0.2841(3)	0.0260(14)
C(15)	0.5912(5)	0.3846(4)	0.2655(2)	0.0227(16)
C(16)	0.5946(4)	0.4157(3)	0.1949(2)	0.0193(12)
C(17)	0.2896(5)	0.4596(3)	−0.1542(2)	0.0197(12)
C(18)	0.2008(6)	0.4484(4)	−0.2211(3)	0.0263(17)
C(19)	0.1908(5)	0.4871(4)	−0.0935(3)	0.0280(16)
C(20)	0.3569(6)	0.3671(3)	−0.1386(3)	0.0277(17)
C(21)	0.9493(5)	0.6779(3)	0.0108(2)	0.0190(12)
C(22)	0.7564(5)	0.7257(3)	0.0912(3)	0.0197(14)
C(23)	0.9352(5)	0.4911(3)	0.0584(3)	0.0253(14)
C(24)	0.9377(6)	0.5937(3)	0.1633(3)	0.0253(16)
C(25)	0.3256(5)	0.2575(3)	0.1065(2)	0.0193(12)
C(26)	0.4087(5)	0.2273(3)	0.0417(3)	0.0290(16)
C(27)	0.2529(6)	0.1727(4)	0.1364(3)	0.0320(17)
C(28)	0.2134(5)	0.3267(3)	0.0833(3)	0.0223(16)

$^a U_{eq} = 1/3\Sigma_i\Sigma_j U_{ij} a_i^* a_j^* a_i \cdot a_j$

salenFeCl [22] but are all slightly elongated by a maximum length of 0.015 Å compared to salenFeCl. The iron nucleus of **1** is situated 0.528(14) Å above the plane defined by the N_2O_2 ligand donor set whereas in salenFeCl the iron atom is lying 0.46 Å above this N_2O_2 plane. Moreover the Cl(1)–Fe(1)–N(2) angle of **1** (105.78(9)) is considerably larger than the corresponding Cl–Fe–N angle of salenFeCl (97.0(3)); this larger angle is probably imposed by the presence of bulky substituents, i.e. the four methyl groups at the ethylene bridge and the tert-butyl groups at the aromatic rings in **1**

Molecular structure of [(L^2)$_2$Fe][BPh$_4$] (2)

X-ray analysis revealed the molecular structure of **2** shown in Fig. 2. The relevant bond lengths and angles are depicted in Table 5. The iron nucleus in complex **2** has a pseudo-octahedral coordination with an N_4O_2

TABLE 3 Fractional atomic coordinates with e.s.d.s in parentheses of the cation of [(L^2)$_2$Fe][BPh$_4$] (**2**)

	x	y	z	B (Å^2)
Fe	0.74135(3)	0.25904(3)	0.76361(3)	1.284(9)
O(2)	0.8060(2)	0.2483(2)	0.6904(2)	1.87(5)
O(19)	0.6246(2)	0.2609(2)	0.6917(2)	1.88(5)
N(10)	0.7362(2)	0.1224(2)	0.7658(2)	1.48(6)
N(18)	0.6900(2)	0.2589(2)	0.8645(2)	1.49(6)
N(27)	0.7439(2)	0.3945(2)	0.7549(2)	1.36(6)
N(35)	0.8720(2)	0.2701(2)	0.8569(2)	1.49(6)
C(3)	0.8389(2)	0.1846(2)	0.6613(2)	1.48(7)
C(4)	0.8924(2)	0.2016(3)	0.6136(2)	1.65(7)
C(5)	0.9243(2)	0.1364(3)	0.5788(2)	1.86(8)
C(6)	0.9035(3)	0.0512(3)	0.5891(2)	2.01(8)
C(7)	0.8523(3)	0.0330(3)	0.6361(2)	1.88(8)
C(8)	0.8201(2)	0.0982(2)	0.6740(2)	1.54(7)
C(9)	0.7683(2)	0.0734(2)	0.7236(2)	1.48(7)
C(11)	0.6849(2)	0.0782(2)	0.8109(2)	1.85(8)
C(12)	0.6051(2)	0.1300(3)	0.8133(2)	1.86(8)
C(13)	0.6288(2)	0.2023(2)	0.8719(2)	1.79(8)
C(14)	0.5919(3)	0.2102(3)	0.9321(3)	2.54(9)
C(15)	0.6169(3)	0.2760(3)	0.9864(2)	2.62(9)
C(16)	0.6801(3)	0.3337(3)	0.9791(2)	2.03(8)
C(17)	0.7140(2)	0.3227(3)	0.9179(2)	1.66(8)
C(20)	0.5698(2)	0.3212(3)	0.6552(2)	1.50(7)
C(21)	0.4844(2)	0.2983(3)	0.6071(2)	1.79(8)
C(22)	0.4264(3)	0.3602(3)	0.5656(2)	2.16(8)
C(23)	0.4510(3)	0.4459(3)	0.5692(3)	2.7(1)
C(24)	0.5344(3)	0.4691(3)	0.6164(2)	2.35(9)
C(25)	0.5947(2)	0.4080(2)	0.6607(2)	1.55(7)
C(26)	0.6800(2)	0.4388(2)	0.7086(2)	1.55(7)
C(28)	0.8246(2)	0.4430(2)	0.7958(2)	1.69(8)
C(29)	0.9073(2)	0.3974(2)	0.7917(2)	1.72(8)
C(30)	0.9350(2)	0.3239(2)	0.8489(2)	1.42(7)
C(31)	1.0229(2)	0.3123(3)	0.8936(2)	1.68(7)
C(32)	1.0466(2)	0.2458(3)	0.9472(2)	1.88(8)
C(33)	0.9813(2)	0.1936(3)	0.9580(2)	1.80(8)
C(34)	0.8955(2)	0.2077(2)	0.9112(2)	1.66(8)

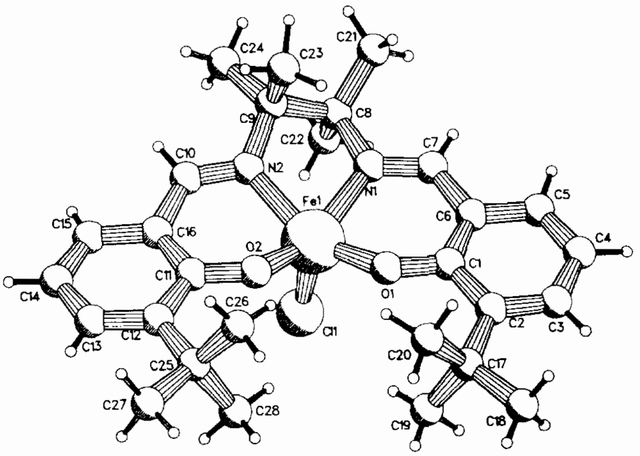

Fig 1 PLUTO drawing of [(L^1)FeCl] (**1**) with adopted numbering scheme

TABLE 4. Selected bond lengths (Å) and bond angles (°) for $[(L^1)FeCl]$ (**1**) with e s d.s in parentheses

Fe(1)–Cl(1)	2.2425(13)	Fe(1)–O(1)	1.886(3)
Fe(1)–O(2)	1.895(3)	Fe(1)–N(1)	2.103(3)
Fe(1)–N(2)	2.079(3)	Cl(1)–Fe(1)–O(1)	106.55(9)
Cl(1)–Fe(1)–O(2)	102.45(9)	Cl(1)–Fe(1)–N(1)	107.50(9)
Cl(1)–Fe(1)–N(2)	105.78(9)	O(1)–Fe(1)–O(2)	94.37(12)
O(1)–Fe(1)–N(1)	86.33(13)	O(1)–Fe(1)–N(2)	146.67(13)
O(2)–Fe(1)–N(1)	148.52(12)	O(2)–Fe(1)–N(2)	86.45(12)
N(1)–Fe(1)–N(2)	76.41(12)	Fe(1)–O(1)–C(1)	133.7(3)

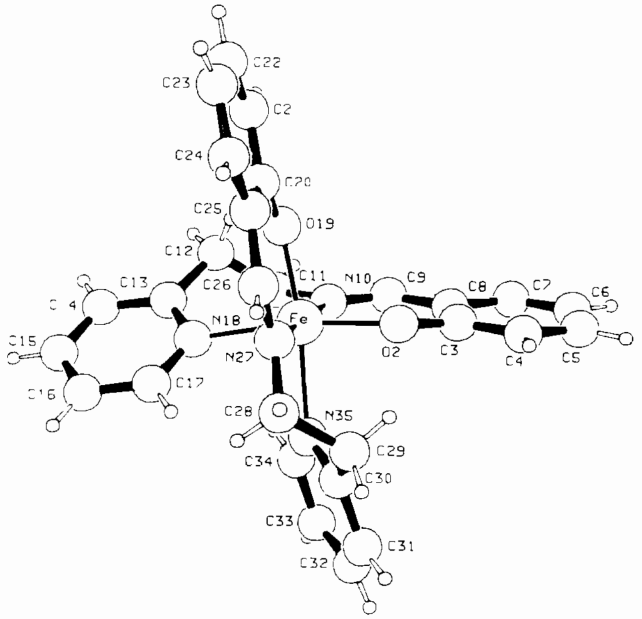

Fig. 2. Molecular structure of the cation of $[(L^2)_2Fe][BPh_4]$ (**2**) with adopted numbering scheme

TABLE 5 Selected bond lengths (Å) and bond angles (°) for $[(L^2)_2Fe][BPh_4]$ (**2**) with e s.d s in parentheses

Fe–O(2)	1.907(3)	Fe–O(19)	1.898(2)
Fe–N(10)	2.138(3)	Fe–N(18)	2.195(3)
Fe–N(27)	2.124(3)	Fe–N(35)	2.224(3)
O(2)–Fe–O(19)	99.9(1)	O(2)–Fe–N(10)	87.5(1)
O(2)–Fe–N(18)	168.5(1)	O(2)–Fe–N(27)	90.7(1)
O(2)–Fe–N(35)	86.1(1)	O(19)–Fe–N(10)	89.6(1)
O(19)–Fe–N(18)	90.5(1)	O(19)–Fe–N(27)	88.4(1)
O(19)–Fe–N(35)	172.3(1)	N(10)–Fe–N(18)	87.6(1)
N(10)–Fe–N(27)	177.0(1)	N(10)–Fe–N(35)	95.5(1)
N(18)–Fe–N(27)	94.6(1)	N(18)–Fe–N(35)	84.1(1)
N(27)–Fe–N(35)	86.7(1)		

ligand donor set; both the two phenolate oxygens as well as the two pyridine nitrogens have a *cis* relationship whereas the two imine nitrogens have a *trans* relationship. The deviation from a perfect octahedral coordination is best illustrated by the O(2)–Fe–N(18) angle (168.5°) and the O(19)–Fe–N(35) angle (172.3°) which markedly deviate form a ideal octahedron (180°). The average Fe–N(pyridine) bond length (2.210 Å) is longer than the average Fe–N(imine) bond length (2.131 Å). The average Fe–O length (1.903 Å), Fe–N(pyridine) length (2.210 Å) and Fe–N(imine) length (2.131 Å) are in accordance with the values reported for structurally related Fe(III) complexes with an N_4O_2 ligand donor set [23–27].

UV–Vis absorption spectra

The most important features of the UV–Vis spectra of complexes **1** and **2** are the low energy bands at 493 nm ($\epsilon = 5020$ l mol^{-1} cm^{-1}) for **1** and 576 nm ($\epsilon = 4460$ l mol^{-1} cm^{-1}) for **2**. These bands are relatively intense and can be assigned to charge transfer transitions from the p_π orbitals of the phenolic oxygens to the d_π^* orbitals of the Fe(III) ions [1, 2, 28] The low energy band of 1 is shifted towards longer wavelength ($\lambda_{max} = 493$ nm) compared to Fe(salen)Cl ($\lambda_{max} = 463$ nm) [22]; this shift to lower energy is probably a result of the difference in the average oxygen–iron distance between the two complexes (see molecular structure of **1**).

For complex **2** the absorption maximum ($\lambda_{max} = 576$ nm) in the visible region lies considerably lower in energy than in the majority of structurally analogous cationic iron(III) complexes with an O_2N_4 ligand donor set; the absorption maxima of reported structurally related iron(III) complexes usually lie in the range 430–540 nm [1, 3, 29, 30].

Cyclic voltammetry

Complex **1** shows a quasi-reversible redox couple at $E_{1/2} = -0.37$ V (versus SCE) in methanol (see Fig. 3) This redox couple is assigned to the Fe(II)/Fe(III) process in analogy with structurally closely related iron(III) salen type ligands [3]. For complex **2** the Fe(II)/Fe(III) redox couple is observed at less negative

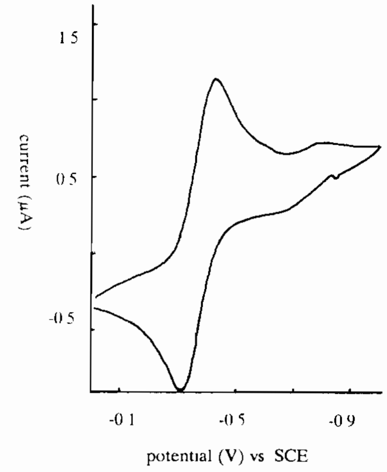

Fig 3 Cyclic voltammogram of $[(L^1)FeCl]$ (1) measured in methanol containing 0.1 M TBAP

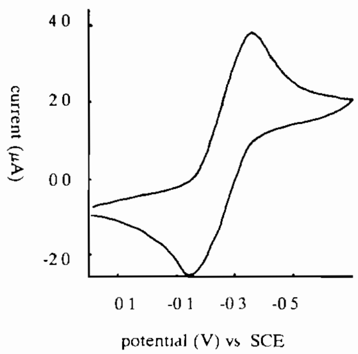

Fig 4 Cyclic voltammogram of $[(L^2)_2Fe][BPh_4]$ (**2**) measured in methanol/acetonitrile (1/1) containing 0.1 M TBAP.

potential: $E_{1/2} = -0.25$ V (versus SCE) in methanol/acetonitrile (1/1) (see Fig. 4).

Discussion

The electrochemical data and the data obtained from the UV–Vis absorption spectra are consistent with observations made by Que and co-workers [3]. It was reported that a relationship exists in the ^1H NMR spectra between the absorption maxima of the phenolate-to-iron charge-transfer transitions and the NMR contact shifts of the salen phenylic hydrogens. This has been explained by delocalization of unpaired spin density onto the ligand. A clear correlation between the electrochemical potentials of the Fe(III)/Fe(II) redox couple and the same ^1H NMR data is also present. Therefore, the electrochemical potentials and absorption maxima are interrelated as well. A plot of the redox potentials versus the UV–Vis absorption maxima, including data of other, related, compounds is shown in Fig. 5.

As is clear from the relationship shown, the absorption maxima of compounds **1** and **2** correlate well with those of the systems reported previously [3]. This correlation has been explained by assuming that the d_π* orbitals of the iron(III) center determine the redox potential as the phenolate-to-iron charge transfer transition is mainly determined by the position of the d_π* orbital (assuming relatively insensitive phenolate p_π orbitals).

Interestingly, the molecular structure of **1** has revealed that the Fe–O and Fe–N distances are significantly longer than those observed for the unsubstituted salen analogue. The steric effects of the bulky tert-butyl groups and the extra methyl groups on the salen ligand cause this elongation of the metal–ligand bond lengths. This elongation of the metal–ligand bond lengths is reflected in the electronic and electrochemical properties; the weaker ligand-field strength causes a less negative reduction potential and concomitantly a lower energy $p_\pi \rightarrow d_\pi^*$ transition.

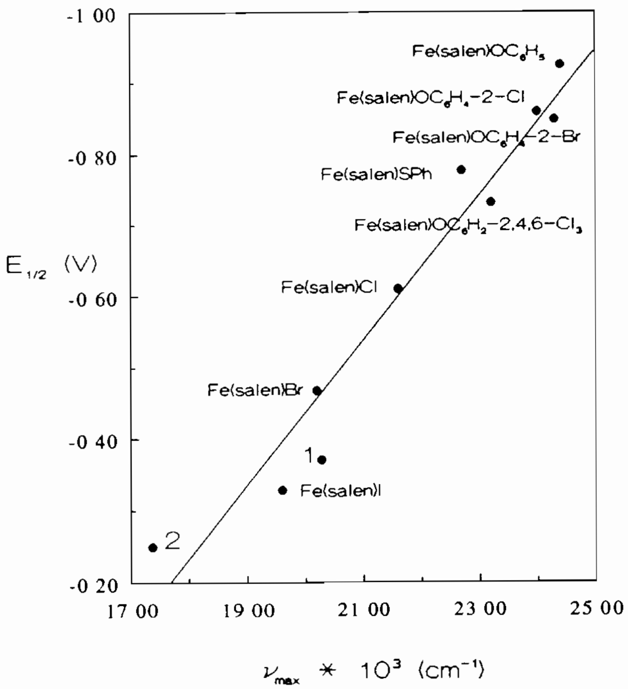

Fig 5. Plot of the Fe(II)/Fe(III) redox potentials vs. the absorption maxima of complexes **1** and **2** and other related complexes.

In conclusion, we have reported the synthesis, crystal and molecular structure as well as UV–Vis spectral data and electrochemical data of two new salen based iron(III) complexes. In our view, these data which combine a detailed structural analysis of **1** and **2** with their UV–Vis spectroscopic properties and electrochemical behavior, should contribute to a better understanding of iron-tyrosinate proteins

Acknowledgement

The financial support of this research by Unilever Research, Vlaardingen, Netherlands, is gratefully acknowledged.

References

1 E W Ainscough, A.M Brodie, J E Plowman, K.L. Brown, A.W Addison and A Ross Gainsford, *Inorg Chem*, *19* (1980) 3655

2 B P. Gaber, V Miskowski and T G. Spiro, *J Am Chem Soc*, *96* (1974) 6868

3 J W Pyrz, A.L Roe, L J. Stern and L. Que, Jr., *J Am. Chem. Soc*, *107* (1985) 614

4 L. Que, Jr, R H Heistand II, R. Mayer and A.L. Roe, *Biochemistry, 19* (1980) 2588.

5 R H Heistand II, R.B. Lauffer, E. Fikrig and L. Que, Jr, *J Am Chem Soc*, *104* (1982) 2789

6 H.G Jang, D.D Cox and L Que, Jr, *J Am Chem Soc*, *113* (1991) 9200

7 B.A Averill, J.C Davis, S. Burman, T. Zirino, J. Sanders-Loehr, T M Loehr, J.T Sage and P.G. Debrunner, *J Am Chem Soc., 109* (1987) 3760.

8 M. Lubben and B L. Feringa, *Inorg Chem,* submitted for publication

9 R.N. Mukherjee, T D.P Stack and R.H. Holm, *J Am. Chem Soc, 110* (1988) 1850.

10 M.L Duran, A Rodriquez, J Romero and A. Sousa, *Synth React Inorg Met -Org Chem., 17* (1987) 681

11 (a) F. van Bolhuis, *J Appl Crystallogr., 4* (1971) 263; (b) G.J.H. van Nes and F. van Bolhuis, *J Appl Crystallogr, 11* (1978) 206.

12 G M. Sheldrick, *SHELXS86,* program for crystal structure solution. University of Gottingen, Germany, 1986.

13 R. Olthof-Hazekamp, CRYLSQ, in S.R Hall and J M. Stewart (eds), *XTAL3.0 User's Manual,* Universities of Western Australia and Maryland, Lamb, Perth, Australia, 1990

14 D.T Cromer and J.B. Mann, *Acta Crystallogr, Sect. A, 24* (1968) 321

15 D.T Cromer and D. Liberman, *J Chem Phys., 53* (1970) 1891.

16 S.R. Hall and J.M. Stewart (eds.), *XTAL3 0 Reference Manual,* Universities of Western Australia, Australia, and Maryland, USA, 1990

17 A.L Spek, *Acta Crystallogr., Sect A, 46* (1990) C-34.

18 (a) A. Meetsma, Extended version of the program PLUTO, University of Groningen, Netherlands, 1991, unpublished, (b) W D S Motherwell and W. Clegg, *PLUTO,* program for plotting molecular and crystal structures University of Cambridge, UK, 1978, unpublished.

19 *Computer Software SDP/PDP,* Enraf-Nonius and B.A. Frenz and Associates, Inc

20 D.T. Cromer and J.T. Waber, *International Tables for X-ray Crystallography,* Vol. IV, Kynoch, Birmingham, UK, 1974, Table 2 2B

21 D T Cromer, *International Tables for X-ray Crystallography,* Vol IV, Kynoch, Birmingham, UK, 1974, Table 2.3 1

22 M. Gerloch and F E. Mabbs, *J. Chem Soc A,* (1967) 1598.

23 B.J. Kennedy, A C. McGrath, K.S. Murray, B.W. Skelton and A.H. White, *Inorg Chem, 26* (1987) 483

24 M.D. Timken, C E Strouse, S.M. Soltis, S.A Daverio, D.N Hendrickson, A.M Abdel-Mawgoud and S R. Wilson, *J. Am. Chem Soc., 108* (1986) 395.

25 Y. Maeda, H Oshio, Y Takashima, M Mikuriya and M. Hidaka, *Inorg Chem, 25* (1986) 2958

26 M.D. Timken, D.N. Hendrickson and E. Sinn, *Inorg Chem., 24* (1985) 3947.

27 Y Maeda, H. Oshio, K. Toriumi and Y Takashima, *J Chem Soc, Dalton Trans,* (1991) 1227.

28 C Flassbeck and K Wieghardt, *Z. Anorg Allg Chem, 608* (1992) 60

29 A.R. Amundsen, J Whelan and B. Bosnich, *Inorg Chem, 18* (1979) 206.

30 Y. Nishida, S Oshio and K. Kida, *Bull Chem Soc Jpn, 50* (1977) 119